

Electromagnetically induced transparency and electromagnetically induced absorption in Y-type system

Kalan Mal, Khairul Islam, Suman Mondal, Dipankar Bhattacharyya, Amitava Bandyopadhyay
Citation: Chin. Phys. B . 2020, 29(5): 054211 . **doi:** 10.1088/1674-1056/ab7ea0
Journal homepage: http://cpb.iphy.ac.cn; http://iopscience.iop.org/cpb

What follows is a list of articles you may be interested in

Dynamic manipulation of probe pulse and coherent generation of beating signals based on tunneling-induced inference in triangular quantum dot molecules

Nuo Ba(巴诺), Jin-You Fei(费金友), Dong-Fei Li(李东飞), Xin Zhong(钟鑫), Dan Wang(王丹), Lei Wang(王磊), Hai-Hua Wang(王海华), Qian-Qian Bao(鲍倩倩)
Chin. Phys. B . 2020, 29(3): 034204 . **doi:** 10.1088/1674-1056/ab683d

Interlayer distance effects on absorption coefficient and refraction index change in p-type double-δ-doped GaAs quantum wells

H Noverola-Gamas, L M Gaggero-Sager, O Oubram
Chin. Phys. B . 2019, 28(12): 124207 . **doi:** 10.1088/1674-1056/ab5278

All-optical switch and transistor based on coherent light-controlled single two-level atom coupling with two nanowires

Xin-Qin Zhang(张新琴), Xiu-Wen Xia(夏秀文), Jing-Ping Xu(许静平), Mu-Tian Cheng(程木田), Ya-Ping Yang(羊亚平)
Chin. Phys. B . 2019, 28(11): 114207 . **doi:** 10.1088/1674-1056/ab48f2

Effect of residual Doppler averaging on the probe absorption in cascade type system: A comparative study

Suman Mondal, Arindam Ghosh, Khairul Islam, Dipankar Bhattacharyya, Amitava Bandyopadhyay
Chin. Phys. B . 2018, 27(9): 094204 . **doi:** 10.1088/1674-1056/27/9/094204

Reflection-type electromagnetically induced transparencyanalogue in terahertz metamaterials

Ding Chun-Feng, Zhang Ya-Ting, Yao Jian-Quan, Sun Chong-Ling, Xu De-Gang, Zhang Gui-Zhong
Chin. Phys. B . 2014, 23(12): 124203 . **doi:** 10.1088/1674-1056/23/12/124203

Electromagnetically induced transparency and electromagnetically induced absorption in Y-type system

Kalan Mal[1,2], Khairul Islam[2], Suman Mondal[2], Dipankar Bhattacharyya[3], and Amitava Bandyopadhyay[2,†]

[1] *Department of Physics, Suri Vidyasagar College, Suri, PIN* 731101, *West Bengal, India*
[2] *Departmet of Physics, Visva-Bharati, Santiniketan, PIN* 731235, *West Bengal, India*
[3] *Department of Physics, Santipur College, Santipur, PIN* 741404, *West Bengal, India*

(Received 19 February 2020; revised manuscript received 3 March 2020; accepted manuscript online 11 March 2020)

The propagation of a probe field through a four-level Y-type atomic system is described in the presence of two additional coherent radiation fields, namely, the control field and the coupling field. An expression for the probe response is derived analytically from the optical Bloch equations under steady state condition to study the absorptive properties of the system under probe field propagation through an ensemble of stationary atoms as well as in a Doppler broadened atomic vapor medium. The most striking result is the conversion of electromagnetically induced transparency (EIT) into electromagnetically induced absorption (EIA) as we start switching from weak probe regime to strong probe regime. The dependence of this conversion on residual Doppler averaging due to wavelength mismatch is also shown by choosing the coupling transition as a Rydberg transition.

Keywords: Y-type system, density matrix method, electromagnetically induced transparency (EIT), electromagnetically induced absorption (EIA)

PACS: 42.50.Gy, 32.10.Fn **DOI:** 10.1088/1674-1056/ab7ea0

1. Introduction

Interaction of atom with coherent radiation fields can lead to many interesting physical phenomena like coherent population trapping (CPT),[1–4] electromagnetically induced transparency (EIT),[5–8] electromagnetically induced absorption (EIA),[9,10] lasing without inversion (LWI),[11,12] subluminal and superluminal propagation of light,[13–15] optical delay generation,[16,17] etc. All these phenomena are expected to have useful applications in future optical devices. Since its theoretical prediction[18] and experimental realization,[5] EIT has become one of the most widely studied topics in quantum optics. EIT makes an otherwise absorptive medium transparent to a resonant or near resonant coherent probe field propagating in the presence of a strong control field. Due to steep variation in the group index around an EIT window and subsequent reduction in the group velocity of the probe pulse,[19] EIT has found immense application in optical delay generation,[16,17] stopping and storage of light,[20] etc. All these are expected to form the backbone of future optoelectronic devices, optical communication, all optical logic gates, and quantum computation. Often a dark-state model is used to explain EIT.[6] In bionic systems also, highly efficient energy transfers between donors and acceptor can be modelled by using a dark-state channel.[21] This is useful to understand the phenomenon of photosynthesis. Similar theoretical study on artificial light harvesting by using dimerized Möbius ring has been reported by Xu *et al.*[22] All these point towards the diverse fields of application of quantum interference phenomena.

Phillips and his co-workers[23] first demonstrated storage of light in Rb vapor at $\sim$ 70–90 ℃ by forming an effective three-level Λ type system. The three-level Λ type system has also been used to show sub-Doppler resolution in an inhomogeneously broadened medium under intense control field.[24] Using an indirectly coupled resonator, Wang and his co-workers studied transparency and absorption, theoretically as well as experimentally, modulated by chiral optical states at exceptional points.[25] They also discussed the possibility of using the findings of this study in optical quantum memory devices and optical computation. Agarwal and Harshwardhan[26] demonstrated the inhibition and enhancement of two-photon absorption in a four-level Y type system. They used two counter propagating weak fields in the Ξ formation and then applied a strong control field which is co-propagating with respect to the weak probe field. The control field acts from the intermediate level, which is common to all three fields, to another excited state. They have considered both Doppler free medium as well as Doppler broadened medium. Later, Gao *et al.*[27] showed electromagnetically induced inhibition of two-photon absorption in sodium vapor at 230 ℃ under two-photon resonance condition. Mirza *et al.*[28] demonstrated the effect of the wave vector mismatch on electromagnetically induced transparency in a four-level Y-type system under weak probe propagation in presence of two stronger fields. They compared the probe absorption and EIT line shape for the same propagation constants of the control

†Corresponding author. E-mail: m2amitava@gmail.com
© 2020 Chinese Physical Society and IOP Publishing Ltd

and probe fields with the EIT line shape obtained when the propagation constant of the probe field is smaller than that of the control field. Bharti and Wasan[29] showed the effect of wavelength mismatch on EIT line shape in a Doppler broadened six-level system. They also compared the results of the four-level Y-type system and three-level Ξ type system. Safari *et al.*[30] discussed the absorption and dispersion features of a weak probe field in the presence of two coupling fields under four-level Y configuration in a Doppler free environment. They used a dressed state model to explain the position and strength of each probe absorption peak. Hao *et al.* reported the observation of EIT by exciting a transition to Rydberg state and observed Autler–Towns splitting in a weak radio frequency electric field.[31] As a practical application of EIT, Wang *et al.* reported frequency locking of a laser by using the EIT signal obtained in ^{85}Rb vapor in the presence of magnetic field.[32] Absolute direct frequency measurement of two-photon transition has also been achieved by the multi-peak fitting approach.[33]

In this article, we present an analytical study of the four-level Y type system based on the density operator method. The analytic expression for the probe response is derived without neglecting any term in any power of the control or probe Rabi frequency. This result is used to study the probe absorption feature in the weak probe regime as well as moderate and strong probe regimes as compared to the control field and the coupling field intensities. Under Doppler broadened condition, the simulated probe absorption shows electromagnetically induced absorption when the probe Rabi frequency is of the same order of magnitude as that of the control and coupling Rabi frequencies. Conversion from EIT to EIA is shown to depend on the residual Doppler averaging due to the wavelength mismatch between the probe field and the control or coupling field by choosing one of the excited states as a Rydberg state. In the weak probe regime, splitting of electromagnetically induced transparency is also visible.

2. Theoretical model

The four-level Y-type system under consideration in this article has only one ground energy level ($|1\rangle$), one intermediate energy level ($|2\rangle$), and two upper excited energy levels ($|3\rangle$ and $|4\rangle$). A coherent probe field of Rabi frequency Ω_p and circular frequency ω_p couples $|1\rangle$ with $|2\rangle$. The intermediate state $|2\rangle$ is coupled to $|3\rangle$ and $|4\rangle$ by two different coherent fields, termed as the control field and the coupling field, respectively. The Rabi frequencies of the control field and the coupling field are represented by Ω_c and Ω_r, respectively. The Rabi frequency of an applied field, having amplitude E_x, is defined as $\Omega_x = \frac{\mu_{ij}E_x}{\hbar}$ with $x =$ p, c, or r for the probe field, control field, or coupling field, respectively. μ_{ij} is the transition dipole matrix element corresponding to the transition $|i\rangle \longrightarrow |j\rangle$ (for $i = 1$, $j = 2$; for $i = 2$, $j = 3$, 4). The transitions considered in this work are all dipole allowed transitions. The spontaneous decay paths of population from different excited states are shown by blue dotted lines in Fig. 1. The spontaneous decay rates from $|4\rangle$ to $|2\rangle$ and from $|3\rangle$ to $|2\rangle$ are represented by γ_{42} and γ_{32}, respectively (Fig. 1). γ_{21} stands for the spontaneous decay rate of atoms from $|2\rangle$ to $|1\rangle$ (Fig. 1). The transfer of population between $|4\rangle$ and $|3\rangle$ is dipole forbidden.

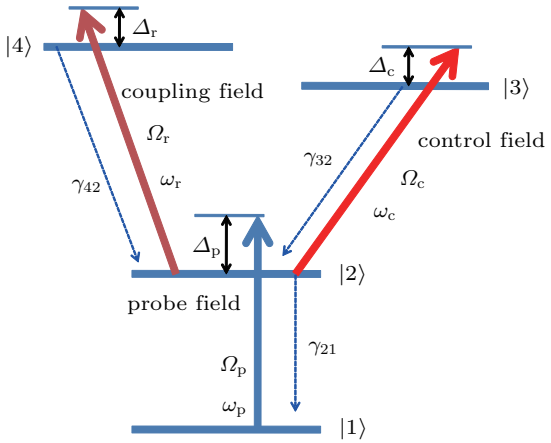


Fig. 1. Level scheme of the Y-type system.

The unperturbed Hamiltonian of the system is given by

$$H_0 = \sum_{i=1}^{4} \hbar\omega_i |i\rangle \langle i| . \tag{1}$$

Here, $E_i = \hbar\omega_i$ (with $i = 1$, 2, 3, 4) is the energy of the i^{th} energy level, $\omega_i = 2\pi\nu_i$. The interaction Hamiltonian is

$$\begin{aligned} H_\mathrm{I} = & -\frac{\hbar\Omega_\mathrm{p}}{2}\left[|2\rangle\langle 1|\,\mathrm{e}^{-\mathrm{i}\omega_\mathrm{p}t} + \mathrm{c.c.}\right] \\ & -\frac{\hbar\Omega_\mathrm{c}}{2}\left[|3\rangle\langle 2|\,\mathrm{e}^{-\mathrm{i}\omega_\mathrm{c}t} + \mathrm{c.c.}\right] \\ & -\frac{\hbar\Omega_\mathrm{r}}{2}\left[|4\rangle\langle 2|\,\mathrm{e}^{-\mathrm{i}\omega_\mathrm{r}t} + \mathrm{c.c.}\right]. \end{aligned} \tag{2}$$

Hence the total Hamiltonian of the system can be written as

$$H_\mathrm{Total} = H_0 + H_\mathrm{I}. \tag{3}$$

After eliminating the time dependent terms by properly choosing the co-rotating frame, the total Hamiltonian can be written in the matrix form as follows:

$$H_\mathrm{Total} = \frac{\hbar}{2}\begin{pmatrix} 0 & -\Omega_\mathrm{p} & 0 & 0 \\ -\Omega_\mathrm{p} & -2\Delta_\mathrm{p} & -\Omega_\mathrm{c} & -\Omega_\mathrm{r} \\ 0 & -\Omega_\mathrm{c} & -2\left(\Delta_\mathrm{p}+\Delta_\mathrm{c}\right) & 0 \\ 0 & -\Omega_\mathrm{r} & 0 & -2\left(\Delta_\mathrm{p}+\Delta_\mathrm{r}\right) \end{pmatrix}. \tag{4}$$

The optical Bloch equations (OBEs) of the four-level Y-type system are derived from the Liouville equation or the Master equation[19] after adding the phenomenological decay terms. These are given as

$$\frac{\partial\rho_{11}}{\partial t} = \frac{\mathrm{i}\Omega_\mathrm{p}}{2}\left(\rho_{21}-\rho_{12}\right) + \gamma_{21}\rho_{22}, \tag{5}$$

$$\frac{\partial\rho_{22}}{\partial t} = -\frac{\mathrm{i}\Omega_\mathrm{p}}{2}(\rho_{21}-\rho_{12})+\frac{\mathrm{i}\Omega_\mathrm{c}}{2}(\rho_{32}-\rho_{23}) + \frac{\mathrm{i}\Omega_\mathrm{r}}{2}(\rho_{42}-\rho_{24})-\gamma_{21}\rho_{22}+\gamma_{32}\rho_{33}+\gamma_{42}\rho_{44}, \quad (6)$$

$$\frac{\partial\rho_{33}}{\partial t} = -\frac{\mathrm{i}\Omega_\mathrm{c}}{2}(\rho_{32}-\rho_{23})-\gamma_{32}\rho_{33}, \quad (7)$$

$$\frac{\partial\rho_{44}}{\partial t} = -\frac{\mathrm{i}\Omega_\mathrm{r}}{2}(\rho_{42}-\rho_{24})-\gamma_{42}\rho_{44}, \quad (8)$$

$$\frac{\partial\rho_{12}}{\partial t} = \left(\Gamma_{21}+\mathrm{i}\Delta_\mathrm{p}\right)\rho_{12}-\frac{\mathrm{i}\Omega_\mathrm{p}}{2}(\rho_{22}-\rho_{11}) + \frac{\mathrm{i}\Omega_\mathrm{c}}{2}\rho_{13}+\frac{\mathrm{i}\Omega_\mathrm{r}}{2}\rho_{14}, \quad (9)$$

$$\frac{\partial\rho_{13}}{\partial t} = \left(\Gamma_{31}+\mathrm{i}\left(\Delta_\mathrm{p}+\Delta_\mathrm{c}\right)\right)\rho_{13}-\frac{\mathrm{i}\Omega_\mathrm{p}}{2}\rho_{23}+\frac{\mathrm{i}\Omega_\mathrm{c}}{2}\rho_{12}, \quad (10)$$

$$\frac{\partial\rho_{14}}{\partial t} = \left(\Gamma_{41}+\mathrm{i}\left(\Delta_\mathrm{r}+\Delta_\mathrm{p}\right)\right)\rho_{14}-\frac{\mathrm{i}\Omega_\mathrm{p}}{2}\rho_{24}+\frac{\mathrm{i}\Omega_\mathrm{r}}{2}\rho_{12}, \quad (11)$$

$$\frac{\partial\rho_{23}}{\partial t} = (\Gamma_{32}+\mathrm{i}\Delta_\mathrm{c})\rho_{23}-\frac{\mathrm{i}\Omega_\mathrm{c}}{2}(\rho_{33}-\rho_{22}) - \frac{\mathrm{i}\Omega_\mathrm{p}}{2}\rho_{13}-\frac{\mathrm{i}\Omega_\mathrm{r}}{2}\rho_{43}, \quad (12)$$

$$\frac{\partial\rho_{24}}{\partial t} = (\Gamma_{42}+\mathrm{i}\Delta_\mathrm{r})\rho_{24}-\frac{\mathrm{i}\Omega_\mathrm{r}}{2}(\rho_{44}-\rho_{22}) - \frac{\mathrm{i}\Omega_\mathrm{p}}{2}\rho_{14}-\frac{\mathrm{i}\Omega_\mathrm{c}}{2}\rho_{34}, \quad (13)$$

$$\frac{\partial\rho_{34}}{\partial t} = (\Gamma_{43}+\mathrm{i}(\Delta_\mathrm{r}-\Delta_\mathrm{c}))\rho_{34}-\frac{\mathrm{i}\Omega_\mathrm{c}}{2}\rho_{24}+\frac{\mathrm{i}\Omega_\mathrm{r}}{2}\rho_{32}. \quad (14)$$

Here, the detunings of the probe, control, and coupling fields under Doppler free condition are defined as $\Delta_\mathrm{p}=\nu_\mathrm{p}-\nu_{21}$, $\Delta_\mathrm{c}=\nu_\mathrm{c}-\nu_{32}$, and $\Delta_\mathrm{r}=\nu_\mathrm{r}-\nu_{42}$, respectively. Furthermore, $\nu_{kl}=\nu_k-\nu_l$ with $k>l$, $k=2$, 3, 4, and $l=1$, 2, 3. The off-diagonal decay rates are represented by Γ_{ij} with $\Gamma_{21}=\frac{\gamma_{21}}{2}$, $\Gamma_{31}=\frac{\gamma_{32}+\gamma_{21}}{2}$, $\Gamma_{32}=\frac{\gamma_{32}+\gamma_{21}}{2}$, $\Gamma_{41}=\frac{\gamma_{42}+\gamma_{21}}{2}$, $\Gamma_{42}=\frac{\gamma_{42}+\gamma_{21}}{2}$, and $\Gamma_{43}=\frac{\gamma_{42}+\gamma_{32}+\gamma_{21}}{2}$. We get sixteen OBEs for this four-level Y-type system out of which we have shown only ten here, but the rest of the equations can be easily obtained by taking the complex conjugation of Eqs. (9)–(14). These equations are solved analytically under steady state condition (i.e., $\partial\rho_{ij}/\partial t=0$ with $i,j=1,2,3,4$) assuming population conservation without neglecting any term in any power of the probe, control, or coupling Rabi frequency to find out an algebraic expression for the probe response term (ρ_{12}),

$$\mathrm{Re}[\rho_{12}] = a_{101}(\rho_{22}-\rho_{11})+a_{102}(\rho_{33}-\rho_{22}) + a_{103}(\rho_{44}-\rho_{22}), \quad (15)$$

$$\mathrm{Im}[\rho_{12}] = a_{98}(\rho_{22}-\rho_{11})+a_{99}(\rho_{33}-\rho_{22}) + a_{100}(\rho_{44}-\rho_{22}). \quad (16)$$

Here a_{ijk} are complicated functions of the Rabi frequencies and detunings of the three fields and the decay rates of population from different energy level. i, j, and k are integers starting from 0 to 9. The absorption and dispersion of the probe field under Doppler free condition are given by

$$\alpha=\frac{4\pi\omega_\mathrm{p}}{c}\mathrm{Im}[\rho_{12}], \quad (17)$$

$$\beta=\frac{4\pi\omega_\mathrm{p}}{c}\mathrm{Re}[\rho_{12}]. \quad (18)$$

Under the Doppler broadened condition, the probe detuning is defined by $\Delta_\mathrm{p}=\nu_\mathrm{p}-\nu_{21}\pm k_\mathrm{p}v$, where v is the velocity of any atom. Similarly, the detunings of the control field and the coupling field are given by $\Delta_\mathrm{c}=\nu_\mathrm{c}-\nu_{32}\mp k_\mathrm{c}v$ and $\Delta_\mathrm{r}=\nu_\mathrm{r}-\nu_{42}\mp k_\mathrm{r}v$, since the control field and the coupling field are taken as counter propagating with respect to the probe field, if not mentioned otherwise. The probe absorption and probe dispersion under Doppler broadened condition are now given by

$$\alpha_D=\int_{-\infty}^{+\infty}M(v)\,\alpha\,\mathrm{d}v, \quad (19)$$

$$\beta_D=\int_{-\infty}^{+\infty}M(v)\,\beta\,\mathrm{d}v. \quad (20)$$

We have assumed that the atoms at temperature T follow the Maxwell's velocity distribution. Here $M(v)=(u\sqrt{\pi})^{-1}\exp\left(-v^2/u^2\right)$ with u representing the most probable velocity of the atoms at temperature T. $u=\sqrt{2k_\mathrm{B}T/m}$ with m being the mass of an atom and k_B the Boltzmann's constant. The value of v can ideally be anything from $-\infty$ to $+\infty$. However we have taken the value of v from -1000 m/s to $+1000$ m/s for simulation.

The perturbation approach can also be used to derive an analytic expression for ρ_{12} by retaining terms linear in Ω_p. The terms containing any power of Ω_c and Ω_r are although retained. This leads to the following expression for $\mathrm{Im}[\rho_{12}]$:

$$\mathrm{Im}[\rho_{12}]=A_1+A_2+A_3. \quad (21)$$

The right hand side of Eq. (21) is a sum of three terms. They are given by

$$A_1 = -\frac{\Omega_\mathrm{p}}{2}\Gamma_{21}\left[\Gamma_{31}^2+\left(\Delta_\mathrm{p}+\Delta_\mathrm{c}\right)^2\right]\left[\Gamma_{41}^2+\left(\Delta_\mathrm{p}+\Delta_\mathrm{r}\right)^2\right] \times\frac{\left[\Gamma_{31}^2+\left(\Delta_\mathrm{p}+\Delta_\mathrm{c}\right)^2\right]\left[\Gamma_{41}^2+\left(\Delta_\mathrm{p}+\Delta_\mathrm{r}\right)^2\right]}{\left(\alpha_1^2+\alpha_2^2\right)}, \quad (22)$$

$$A_2 = -\frac{\Omega_\mathrm{p}}{2}\frac{\Omega_\mathrm{c}^2}{4}\Gamma_{31}\left[\Gamma_{41}^2+\left(\Delta_\mathrm{p}+\Delta_\mathrm{r}\right)^2\right] \times\frac{\left[\Gamma_{31}^2+\left(\Delta_\mathrm{p}+\Delta_\mathrm{c}\right)^2\right]\left[\Gamma_{41}^2+\left(\Delta_\mathrm{p}+\Delta_\mathrm{r}\right)^2\right]}{\left(\alpha_1^2+\alpha_2^2\right)}, \quad (23)$$

$$A_3 = -\frac{\Omega_\mathrm{p}}{2}\frac{\Omega_\mathrm{r}^2}{4}\Gamma_{41}\left[\Gamma_{31}^2+\left(\Delta_\mathrm{p}+\Delta_\mathrm{c}\right)^2\right] \times\frac{\left[\Gamma_{31}^2+\left(\Delta_\mathrm{p}+\Delta_\mathrm{c}\right)^2\right]\left[\Gamma_{41}^2+\left(\Delta_\mathrm{p}+\Delta_\mathrm{r}\right)^2\right]}{\left(\alpha_1^2+\alpha_2^2\right)}, \quad (24)$$

with

$$\alpha_1 = \Gamma_{21}\left[\Gamma_{31}^2+\left(\Delta_\mathrm{p}+\Delta_\mathrm{c}\right)^2\right]\left[\Gamma_{41}^2+\left(\Delta_\mathrm{p}+\Delta_\mathrm{r}\right)^2\right] + \frac{\Omega_\mathrm{c}^2}{4}\Gamma_{31}\left[\Gamma_{41}^2+\left(\Delta_\mathrm{p}+\Delta_\mathrm{r}\right)^2\right] + \frac{\Omega_\mathrm{r}^2}{4}\Gamma_{41}\left[\Gamma_{31}^2+\left(\Delta_\mathrm{p}+\Delta_\mathrm{c}\right)^2\right], \quad (25)$$

$$\alpha_2 = \Delta_p\left[\Gamma_{31}^2+\left(\Delta_p+\Delta_c\right)^2\right]\left[\Gamma_{41}^2+\left(\Delta_p+\Delta_r\right)^2\right] - \frac{\Omega_c^2}{4}\left(\Delta_p+\Delta_c\right)\left[\Gamma_{41}^2+\left(\Delta_p+\Delta_r\right)^2\right] - \frac{\Omega_r^2}{4}\left(\Delta_p+\Delta_r\right)\left[\Gamma_{31}^2+\left(\Delta_p+\Delta_c\right)^2\right]. \quad (26)$$

Clearly, equation (21) contains only linear terms in Ω_p. This expression can be used to study the probe absorption in the four-level Y-type system by putting Eq. (21) in Eq. (17) for a Doppler free environment. Under the Doppler broadened condition, equation (19) has to be used instead of Eq. (17) to investigate the probe response. A comparative study between the perturbative approach [Eq. (21)] and the complete analytical approach [Eq. (16)] will be presented in Subsection 3.2.

3. Results and discussion

3.1. Doppler free condition

We shall first discuss the probe field propagation through the Y-type system under Doppler free condition. The spontaneous decay rate from level $|2\rangle$ to the ground level $|1\rangle$ (γ_{21}) is assigned from Ref. [34], whereas the spontaneous decay rates from levels $|3\rangle$ and $|4\rangle$ (γ_{32} and γ_{42} respectively) to level $|2\rangle$ are taken from Ref. [19]. Figure 2 shows the simulated probe absorption vs. probe detuning at $\Delta_c = 50$ MHz and $\Delta_r = -50$ MHz. The probe Rabi frequency is set at $\Omega_p = 1$ MHz for all the simulations if not mentioned otherwise. The control and coupling Rabi frequencies are given in the inset of Fig. 2. For $\Delta_c \neq \Delta_r$, each set of Ω_c and Ω_r shows two transparency windows due to the two cascade subsystems (one for the control–probe pair and the other for the coupling–probe pair) of the Y-type system. The equal and opposite detunings of the control field and the coupling field produce symmetric double-EIT windows (with respect to Δ_p =0) only for $\Omega_c = \Omega_r$ (blue curve in Fig. 2). Otherwise it will be asymmetric. One interesting feature of the probe absorption profile is that the width of the EIT window caused by the control–probe subsystem with $\Omega_c > \Omega_r$ (red curve in Fig. 2) is greater than that for the same subsystem with $\Omega_c = \Omega_r$ (blue curve in Fig. 2), with the numerical value of Ω_c being the same for both cases. Identical feature is observed for the coupling–probe subsystem with $\Omega_r > \Omega_c$ (black curve in Fig. 2).

The reason for different widths of the EIT windows produced by the control–probe (coupling–probe) subsystem, just shown in Fig. 2 and mentioned above, points towards a cross-talking between the two cascade subsystems of the Y-type system. The transparency window due to the control–probe subsystem can be tuned by varying the detuning and Rabi frequency of the coupling field and vice versa. A semi classical dressed state model is used to determine the eigenstates.[30] Under weak probe approximation ($\Omega_p \ll \Omega_c, \Omega_r$), the characteristic equation obtained by diagonalizing the Hamiltonian in Eq. (4) is given by

$$\lambda\left[\left(2\Delta_p+\lambda\right)\left\{\left(2\Delta_p+\lambda\right)^2+2\left(\Delta_r+\Delta_c\right)\left(2\Delta_p+\lambda\right) +4\Delta_c\Delta_r-\left(\Omega_c^2+\Omega_r^2\right)\right\}-2\left[\Delta_r\Omega_c^2+\Delta_c\Omega_r^2\right]\right]=0. \quad (27)$$

For $\Omega_c = \Omega_r = \Omega$ and $\Delta_r = -\Delta_c = \Delta$, the eigenvalues of the above equation are

$$\lambda_0 = 0, \quad \lambda_1 = -2\Delta_p,$$
$$\lambda_+ = -\sqrt{2}\left[\sqrt{2}\Delta_p - \sqrt{\left(2\Delta^2+\Omega^2\right)}\right],$$
$$\lambda_- = -\sqrt{2}\left[\sqrt{2}\Delta_p + \sqrt{\left(2\Delta^2+\Omega^2\right)}\right].$$

Here, $\lambda_0 = 0$ corresponds to the uncoupled state or dark state. The ground state $|1\rangle$ is the dark state. There will be no absorption of the probe field acting on this state and the population gets trapped here. If the Rabi frequency of the probe field is not negligible compared to the other two fields, an extra term $\Omega_p^2\left\{2\left(\Delta_p+\Delta_c\right)+\lambda\right\}\left\{2\left(\Delta_p+\Delta_r\right)+\lambda\right\}$ will appear on the left hand side of Eq. (27) and the dark state formation ($\lambda_0 = 0$) is hampered. However, for the general case where $\Omega_c \neq \Omega_r$ and $\Delta_r \neq \Delta_c$ it becomes tedious to solve the characteristic equation analytically.

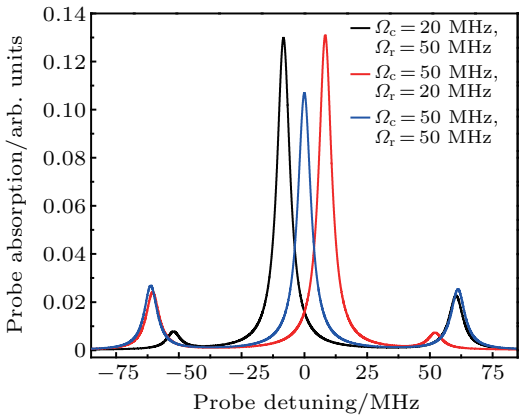


Fig. 2. The probe absorption vs. probe detuning under Doppler free condition. $\Delta_c = 50$ MHz, $\Delta_r = -50$ MHz.

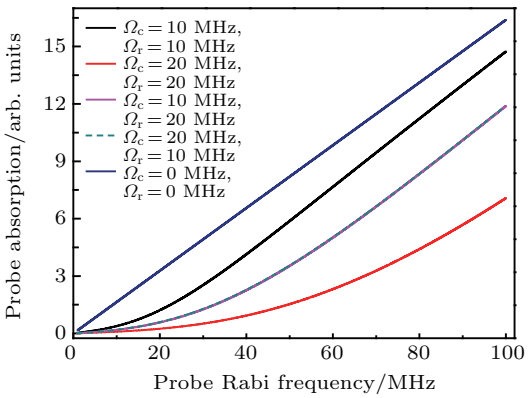


Fig. 3. The probe absorption vs. probe Rabi frequency at $\Delta_p = \Delta_c = \Delta_r = 0$.

Since in deriving the analytical expression for the probe absorption [Eq. (16)] we have not neglected any term in any

power of Ω_p, the expression can be used without any restriction on the relative value of the probe Rabi frequency with respect to the Rabi frequencies of the control and coupling fields. That is why we can study the probe absorption by using this analysis when $\Omega_p \sim \Omega_c, \Omega_r$ or $\Omega_p \geqslant \Omega_c, \Omega_r$. A perturbation approach, which keeps only the linear terms in the probe Rabi frequency and retains terms of any order in coupling and control Rabi frequencies in general, is not useful to study the probe absorption at probe Rabi frequency comparable or higher than the control Rabi frequency and coupling Rabi frequency.[29,30] In Fig. 3, the probe absorption vs. Ω_p at different values of control and coupling Rabi frequencies is plotted. The probe absorption increases linearly with Ω_p for $\Omega_c = \Omega_r = 0$ (solid navy blue line in Fig. 3). It is visible from this figure that the probe transmission through the atomic medium increases at higher values of Ω_c and Ω_r. When the values of the control and coupling Rabi frequencies are interchanged (for $\Omega_c \neq \Omega_r$), the plots of probe absorption vs. probe Rabi frequency coincides with each other (pink curve and dotted blue curve in Fig. 3). At higher values of Ω_c and Ω_r, the trapping of population in the ground state is favored, hence the probe absorption is very small. In that domain, the increase rate of the probe absorption with the probe Rabi frequency stays low. For $\Omega_p \gg \Omega_c, \Omega_r$, the dark state formation is not favored anymore and the probe absorption starts rising fast. This is well in accordance with the dressed state analysis. However, under Doppler free condition, with the control field and the coupling field switched on, we do not observe the probe absorption to shoot above the probe absorption in the absence of the control field and coupling field (Fig. 3). This means that enhanced probe absorption in the presence of the control field and the coupling field does not happen under Doppler free condition. But under Doppler broadened condition, when Ω_p is increased we do observe enhancement in the probe absorption in the presence of the control field and the coupling field as compared to that in the absence of the control and coupling fields. Thus for the Y-type system, a conversion from EIT to enhanced absorption like phenomenon takes place under Doppler broadened condition (Subsection 3.2 (Fig. 6)). The result shown in Fig. 3 can only be studied with the help of an analysis which is free from perturbative approximations since the perturbative model (Eqs. (21)–(26)) is not valid when $\Omega_p \sim \Omega_c, \Omega_r$ or $\Omega_p > \Omega_c, \Omega_r$.

3.2. Doppler broadened condition

We shall now discuss the probe absorption features under Doppler broadened condition ($T = 300$ K). The difference in wavelengths of the three fields substantially modifies the probe absorption line shape as compared to the case where all the three fields are assumed to have the same wavelength.[29,30] The probe absorption in the strong probe field regime will also be studied.

Three different regimes can be conceived of depending on whether the wavelengths of the probe, control, and coupling fields are the same or different.[29] We shall consider a few specific transitions executed by ^{87}Rb to elaborate the situation. The wavelengths of the probe, control, and coupling fields are represented by λ_p, λ_c, and λ_r, respectively. Similarly, the propagation constants of the three fields are designated by k_p, k_c, and k_r with $k_i = 2\pi/\lambda_i$, where $i =$ p, c, or r. The wavelength of the probe field is taken to be $\lambda_p = 780$ nm. We designate the different Y-type transitions of ^{87}Rb as Tr-I, Tr-II, and Tr-III in Table 1.

Table 1. The Y-type transitions in ^{87}Rb.

Transition	Wavelength of the control field	Wavelength of the coupling field
Tr-I:	$\lambda_c = 776$ nm	$\lambda_r = 776$ nm
$^{87}\mathrm{Rb}\ 5S_{1/2} \rightarrow 5P_{3/2} \rightarrow \begin{cases} 5D_{5/2} \\ 5D_{3/2} \end{cases}$	$(5P_{3/2} \rightarrow 5D_{5/2})$	$(5P_{3/2} \rightarrow 5D_{3/2})$
Tr-II:	$\lambda_c = 776$ nm	$\lambda_r = 572$ nm
$^{87}\mathrm{Rb}\ 5S_{1/2} \rightarrow 5P_{3/2} \rightarrow \begin{cases} 5D_{5/2} \\ 7D_{5/2} \end{cases}$	$(5P_{3/2} \rightarrow 5D_{5/2})$	$(5P_{3/2} \rightarrow 7D_{5/2})$
Tr-III:	$\lambda_c = 572$ nm	$\lambda_r = 480$ nm
$^{87}\mathrm{Rb}\ 5S_{1/2} \rightarrow 5P_{3/2} \rightarrow \begin{cases} 7D_{5/2} \\ 44D_{5/2} \end{cases}$	$(5P_{3/2} \rightarrow 7D_{5/2})$	$(5P_{3/2} \rightarrow 44D_{5/2})$

From Table 1, it is evident that in this study we always have $\lambda_p \neq \lambda_c$ and $\lambda_p \neq \lambda_r$. As a result, strictly speaking, no cascade sub-system of the Y-type configuration will be Doppler-free, i.e., $\left(\mp \frac{v}{\lambda_p} \pm \frac{v}{\lambda_c}\right) \neq 0$ and $\left(\mp \frac{v}{\lambda_p} \pm \frac{v}{\lambda_r}\right) \neq 0$ for all the cases to be discussed. However, for Tr-I we have $\left(\mp \frac{v}{\lambda_p} \pm \frac{v}{\lambda_c}\right) = \left(\mp \frac{v}{\lambda_p} \pm \frac{v}{\lambda_r}\right)$. As a result, the two-photon resonance condition will be satisfied simultaneously for both the sub-systems. The residual Doppler broadening will be the least for this transition.

The probe absorption vs. probe detuning for three different transitions (Tr-I, Tr-II, Tr-III) (see Table 1) under Doppler broadened condition is shown in Fig. 4. In the simulation, we have used $\Omega_c = \Omega_r = 10$ MHz and $\Delta_c = \Delta_r = 0$. EIT is formed at $\Delta_p = 0$ in the Doppler broadened probe absorption curves for all the three sets of transitions. The transparency is minimum for Tr-I and maximum for Tr-III. The enhancement

in the transparency is attributed to residual Doppler averaging due to wavelength mismatch for both cascade sub-systems. It is to be noted carefully that the EIT line shape shows splitting for Tr-II (red curve in Fig. 4) where there is a large wavelength mismatch between the control transition and the coupling transition. As a result, $\left(\mp\frac{v}{\lambda_p}\pm\frac{v}{\lambda_c}\right)\neq\left(\mp\frac{v}{\lambda_p}\pm\frac{v}{\lambda_r}\right)$ and the two-photon resonance position changes prominently for different velocity groups of atoms for the two cascade subsystems,[28,29] resulting in two different EIT positions for them and hence the apparent splitting in the transparency profile in Fig. 4. For Tr-III, the residual Doppler averaging due to wavelength mismatch between the two cascade sub-systems of the Y-type system is appreciable. For this transition, the transparency is maximum, although just like Tr-I no splitting in the EIT line profile can be observed. This means when the wavelengths of the control transition and coupling transition are not far apart, we do not get any splitting in the EIT profile.

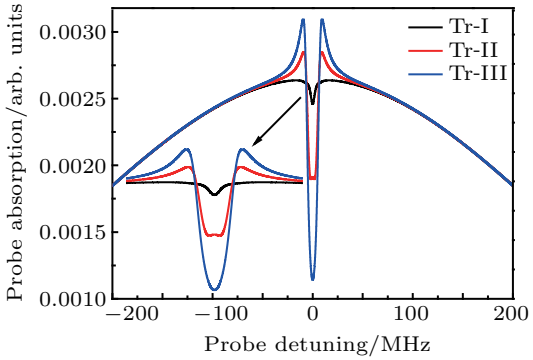


Fig. 4. The probe absorption vs. probe detuning under Doppler broadened condition for three different sets of transitions. $\Omega_c=\Omega_r=10$ MHz and $\Delta_c=\Delta_r=0$.

We shall now show that the perturbative result [Eq. (21)] fails to exhibit some features that can only be obtained through the comprehensive analytical treatment [Eq. (16)].

Figure 5 shows the simulated probe absorption obtained by using the perturbation free analytical model [Eq. (16)] (black curve) as well as by using the perturbative model [Eqs. (21)–(26)] (red curve) at $\Omega_p=10$ MHz, $\Omega_c=\Omega_r=20$ MHz. Henceforth we shall term the first model as model-1 and the second model as model-2. There is some difference between the results of these two models. The horn like structures on either side of the EIT window, as can be observed in the plot obtained by using model-2 (red curve in Fig. 5), are absent when we use model-1 (black curve in Fig. 5). The reason for this discrepancy is the omission of the higher order terms in Ω_p in the perturbative treatment. This introduces some artifact in the result. This deviation is enhanced when the value of Ω_p is increased further. The analytical expression of the probe coherence term can be written as the summation of three different terms as shown in Eqs. (21)–(24). It can easily be verified that the splitting in the EIT window is due to the second term (term-2, Eq. (23)) which is proportional to the square of the Rabi frequency of the control field. This term is also plotted in Fig. 5 (the magenta curve). As we set $\Omega_p\sim\Omega_c$, the transparency at $\Delta_p=0$ cannot be formed anymore, rather enhancement in absorption can be noticed. This is due to obstruction in dark state formation at $\Delta_p=0$ in the ground state at high values of Ω_p in the presence of the different velocity groups of atoms. It is to be remembered that these are all for Tr-II where there is difference in residual Doppler averaging due to wavelength mismatch between the control–probe subsystem and the coupling–probe subsystem.

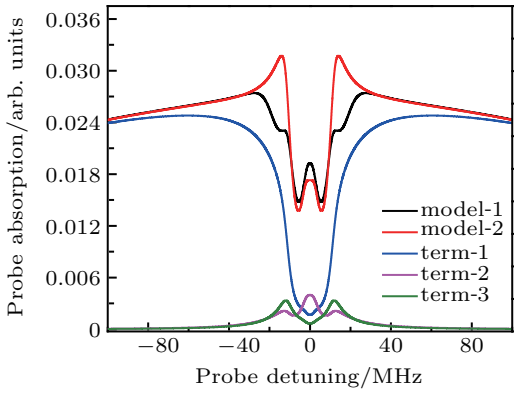


Fig. 5. The probe absorption vs. probe detuning by using model-1 and model-2. $\Omega_p=10$ MHz, $\Omega_c=\Omega_r=20$ MHz.

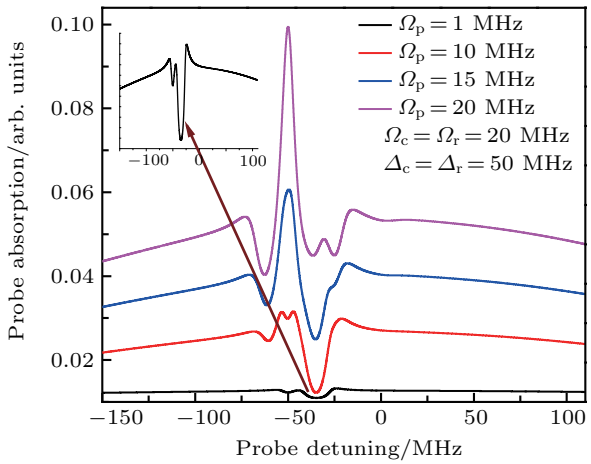


Fig. 6. The probe absorption vs. probe detuning at different Ω_p.

If the control and coupling fields are both detuned by equal amount, say +50 MHz, the EIT windows produced by the control–probe pair and the coupling–probe pair get separated (Fig. 6). The propagation constants of the coupling and probe fields for Tr-II largely differ from each other although those of the control and probe fields are very close to each other; hence under velocity averaging the position of the two-photon resonance for the coupling–probe sub-system differs from that due to the control–probe pair. As a result, the EIT windows corresponding to the two sub-systems are produced at different values of probe detuning (Fig. 6). As the probe Rabi frequency is increased, the depth of the EIT window due to the control–probe pair decreases faster and turns

into an enhanced absorption like feature (compare the plots of Fig. 6). However, for the coupling–probe pair, this does not happen so easily. Thus, the residual Doppler averaging due to wavelength mismatch also plays its part in preventing the transformation of the EIT window into an EIA type feature as Ω_p is increased. By tuning the Rabi frequency of the probe field it is possible to fine control the EIT and EIA windows and their conversion. In Fig. 6, at $\Omega_c = \Omega_r = 20$ MHz and $\Omega_p = 10$ MHz, the control–probe pair shows EIA type feature alongside the EIT window caused by the coupling–probe pair. At $\Omega_p = 15$ MHz, the depth of the transparency window decreases and the EIA gets enhanced. At $\Omega_p = 20$ MHz, the transparency decreases further with a peak forming at its middle for the coupling–probe pair, whereas the EIA keeps getting stronger for the control–probe pair. The trapping of population is badly hampered for $\Omega_p \sim \Omega_c, \Omega_r$ and this destroys EIT. Increasing the Rabi frequency of the probe field further turns the transparency window due to the coupling–probe sub-system into EIA, just like the control–probe sub-system. Hence for the highly excited Rydberg transition, the probe field needs to be of greater intensity to convert the EIT window into an EIA type feature as compared to the low lying excited state for the control transition.

Moon and his co-worker have showed the conversion of two-photon absorption (TPA) to three-photon electromagnetically induced absorption (TPEIA) and two-photon EIT to TPEIA using ^{87}Rb $5S_{1/2} \rightarrow 5P_{3/2} \rightarrow 5D_{5/2}$ transition.[35] The wavelengths of the control and probe lasers used there are identical to Tr-I in Table 1. The usual counter-propagating control–probe configuration results in EIT or TPA depending on the decay of population between the ground and intermediate states.[35] Introduction of an additional coupling beam, counter-propagating with respect to the control beam and having the same wavelength (776 nm) as that of the control beam, transforms EIT and TPA into TPEIA. They have also analyzed the experimental findings by using a numerical model and simulated the formation of TPEIA in two-photon EIT as well as in TPA. In that work,[35] the control and probe laser beams have a fixed intensity. In the present work, we have shown the conversion of EIT into EIA by varying the probe intensity where the probe is counter-propagating relative to both the control and coupling fields under Y-configuration. The strength of the EIA peak produced due to the control–probe sub-system is found to depend on the interference between the coupling and control transitions. The EIA peak is found to be the strongest when the coupling–probe resonance is far detuned from the control–probe pair. The basic difference is that whereas in Ref. [35] the coupling and control fields are both exciting the same $5P_{3/2} \rightarrow 5D_{5/2}$ multiplate, in this article the coupling and control fields have been used to excite two completely different transition pathways from the $5P_{3/2}$ level. We have not noticed any conversion from TPA to three-photon EIA.

4. Conclusion and perspectives

We have emphasized on the analytical solution for the probe response in the four-level Y-type configuration. The solution has been obtained without any simplistic approximation like weak probe field relative to the other two radiation fields. The result obtained by this model is also compared with the perturbative solution. It is clearly shown that the residual Doppler averaging due to wavelength mismatch between the control or coupling field and the probe field plays a crucial role in the formation of EIT window under Doppler broadened condition. It has also been demonstrated that under Doppler free condition the probe absorption vs. probe detuning shows identical variation when unequal values of control and coupling Rabi frequencies are interchanged. This is not true under Doppler broadened condition due to residual Doppler averaging. In this model, the freedom of choosing the intensity of the probe field comparable to the intensities of the control and coupling fields makes the study very different from the usual perturbative approach. Since both EIT and EIA can now be created in the same Doppler broadened absorption window, we can have opposite dispersions for EIT and EIA within the same absorption profile. This would result in sub-luminal and super-luminal propagation of the probe field within one absorption window. This points towards possible application in optical switching and the switching windows can be tuned by adjusting the detunings and the intensities of the control and coupling fields. The nature of switching can be easily reversed by playing with the intensity of the probe field too, if one does not want to tune the intensities of the two other fields.

Acknowledgments

KM acknowledges UGC (ERO) for granting a minor research project (F. No. PSW: 050(2015–16), date-16/11/2016). SM acknowledges UGC (New Delhi) for providing research fellowship (JRF-NET, vide sanction No. F.17-124/2008(SA-I) dated 22/08/2014). DB acknowledges SERB for granting a project under Teaching Associateship for Research Excellence (TARE) scheme (sanction no. TAR/2018/000710). AB acknowledges the University Grants Commission (New Delhi) for sanctioning a major research project (F. No - 43–527/2014(SR) dated 28/09/2015).

References

[1] Agap'ev B D, Gornyĭ M B, Matisov B G and Rozhdestvenskiĭ Y V 1993 *Phys.-Usp.* **36** 763
[2] Zhao S M and Zhuang P 2014 *Chin. Phys. B* **23** 054203
[3] Zhang Y, Qu S and Gu S 2012 *Opt. Express* **20** 6400
[4] Qu S P, Zhang Y and Gu S H 2013 *Chin. Phys. B* **22** 099501
[5] Boller K J, Imamoglu A and Harris S E 1991 *Phys. Rev. Lett.* **66** 2593

[6] Harris S E 1997 *Phys. Today* **50** 36
[7] Jiang X, Zhang H and Wang Y 2016 *Chin. Phys. B* **25** 034204
[8] Cheng H, Wang H M, Zhang S S, Xin P P, Luo J and Liu H P 2017 *Opt. Exp.* **25** 33575
[9] Lezama A, Barreiro S and Akulshin A M 1999 *Phys. Rev. A* **59** 4732
[10] Zhao Y T, Zhao J M, Xiao L T, Yin W B and Jia S T 2004 *Chin. Phys. Lett.* **21** 76
[11] Agarwal G S 1991 *Phys. Rev. A* **44** R28
[12] Hamedi H R, Juzeliūnas G, Raheli A and Sahrai M 2013 *Opt. Commun.* **311** 261
[13] Agarwal G S, Dey T N and Menon S 2001 *Phys. Rev. A* **64** 053809
[14] Zhang Q, Qu G H, Tang Y H, Jin K and Ji W L 2012 *Chin. Phys. B* **21** 023201
[15] Mondal S, Ghosh A, Islam K and Bandyopadhyay A 2019 *Laser Phys.* **29** 075204
[16] Yan L S, Lin L, Belisle A, Wey S and Yao X S 2007 *J. Opt. Network.* **6** 13
[17] Novikova I, Phillips D F and Walsworth R L 2007 *Phys. Rev. Lett.* **99** 173604
[18] Harris S E, Field J E and Imamoglu A 1990 *Phys. Rev. Lett.* **64** 1107
[19] Mondal S, Ghosh A, Islam K and Bandyopadhyay A 2019 *Opt. Commun.* **435** 378
[20] Heinze G, Hubrich C and Halfmann T 2013 *Phys. Rev. Lett.* **111** 033601
[21] Dong H, Xu D Z, Huang J F and Sun C P 2012 *Light: Sci. & Appl.* **1** e2
[22] Xu L, Gong Z R, Tao M J and Ai Q 2018 *Phys. Rev. E* **97** 042124
[23] Phillips D F, Fleischhauer A, Mair A and Walsworth R L 2001 *Phys. Rev. Lett.* **86** 783
[24] Vemuri G, Agarwal G S and Nageswara Rao B D 1996 *Phys. Rev. A* **53** 2842
[25] Wang C, Jiang X, Zhao G, Zhang M, Hsu C W, Peng B, Stone A D, Jiang L and Yang L 2020 *Nat. Phys.*
[26] Agarwal G S and Harshawardhan W 1996 *Phys. Rev. Lett.* **77** 1039
[27] Gao J Y, Yang S H, Wang D, Guo X Z, Chen K X, Jiang Y and Zhao B 2000 *Phys. Rev. A* **61** 023401
[28] Mirza A B and Singh S 2012 *Phys. Rev. A* **85** 053837
[29] Bharti V and Wasan A 2014 *Opt. Commun.* **324** 238
[30] Safari L, Iablonskyi D and Fratini F 2014 *Eur. Phys. J. D* **68** 27
[31] Hao L, Xue Y, Fan J, Jiao Y, Zhao J and Jia J 2019 *Chin. Phys. B* **28** 053202
[32] Wang H M, Cheng H, Zhang S S, Xin P P, Xu Z S and Liu H P 2018 *Chin. Phys. B* **27** 094205
[33] Dai S, Li K, Zhai Y, Xia W, Wang Q, Xiong W, Qi X and Chen X 2017 *Chin. Phys. Lett.* **34** 13201
[34] Steck D A 2015 Rubidium 87 D line data version 2.1.5 2015
[35] Moon H S and Jeong T 2014 *Phys. Rev. A* **89** 033822